

pubs.acs.org/JPCC Article

Quantum Mechanical Effects in High-Resolution Tip-Enhanced Raman Imaging

Published as part of The Journal of Physical Chemistry virtual special issue "Nanophotonics for Chemical Imaging and Spectroscopy".

Rebecca L. M. Gieseking*



Cite This: J. Phys. Chem. C 2022, 126, 11690-11700



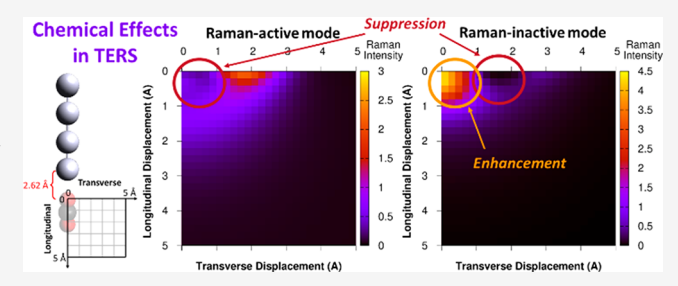
ACCESS

III Metrics & More

Article Recommendations

s Supporting Information

ABSTRACT: Tip-enhanced Raman spectroscopy (TERS) with atomically sharp tips can achieve subnanometer spatial resolution due to confinement of the plasmonic electric field. Although enhancement of the local electromagnetic field is generally the dominant enhancement mechanism, chemical interactions may substantially modify the TERS intensity on the subnanometer scale. Modeling these chemical interactions requires a quantum mechanical treatment of both the molecule and the metal tip. The semiempirical INDO/CIS model reproduces the TD-DFT optical spectra of Ag nanoclusters and allows straightforward decom-



position of the TERS enhancement into electromagnetic and chemical contributions. In a prototypical Ag_n nanowire— CO_2 system, we show that chemical interactions on a subnanometer scale substantially modify the TERS intensity, suppressing the signal of the Raman-active stretching mode and enhancing the signal of the Raman-inactive mode. The enhancement profile in the TERS images results from changes in three distinct factors: (1) the effective electric field on the nanowire, (2) the extent of ground-state charge transfer, and (3) the extent of mixing between σ -type and π -type molecular orbitals due to symmetry-breaking. These results suggest that a subtle interplay between several quantum mechanical effects are critical to understand the origins of TERS images on the subnanometer scale.

1. INTRODUCTION

Tip-enhanced Raman spectroscopy (TERS) is a powerful tool to study chemical systems within a localized environment. ¹⁻³ In TERS, excitation of the plasmon resonance of a sharp tip, typically composed of a noble metal like silver or gold, causes strong enhancement of the Raman intensity of molecular vibrations. In recent years, atomically sharp tips have enabled vibrational imaging of single molecules on surfaces with subnanometer resolution. ^{2,4-6} As the tip is moved laterally across a molecule, the Raman spectrum changes: different vibrational modes are enhanced at different tip positions above the molecule, ⁵ and the selection rules that determine which modes are Raman-active change substantially from those for the isolated molecule. ⁶

The fundamental enhancement mechanisms of the Raman signal in TERS are the same as those in surface-enhanced Raman spectroscopy (SERS). The electromagnetic mechanism (EM), based on enhancement on the local electric fields, typically makes the largest contribution to the overall enhancement factor (EF) and can be on the order of $10^7 - 10^{10}$ in hot spots. The chemical mechanism (CM) is usually a smaller contribution to the EF, on the order of $10^1 - 10^3$. This mechanism includes two closely related effects: (1) the ground-state (GS)

mechanism, based on changes to the electronic ground state due to interactions between the molecule and the tip, and (2) the charge-transfer (CT) mechanism, where the resonance of charge-transfer excited states with the incoming light lead to enhancement of the Raman signal.

To date, most modeling of these TERS images has focused on the EM enhancement, using a hybrid discrete interaction model/quantum mechanics (DIM/QM) to capture the classical electric field of an atomistic TERS tip on a Raman-active molecule that is described quantum mechanically. For porphyrin-like molecules, this model can produce TERS images in qualitative agreement with experiments, and the resolution is highly sensitive to the tip—molecule distance. The gradient of the electric field across the molecule can also significantly modify the EF at these scales due to local symmetry breaking. These field gradient effects cause the relaxation of

Received: May 12, 2022 **Revised:** June 30, 2022 **Published:** July 12, 2022





the selection rules seen experimentally. However, electrodynamics models of the TERS tips cannot describe the contribution of the CM to the overall enhancement.

Quantum mechanical (QM) modeling of the TERS tip can give insight into the CM enhancement that is not feasible using electrodynamics models. For SERS, models of the tip-molecule complex based on density functional theory (DFT) have shown that both the EM and the CM contribute to the total SERS enhancement. 18 This enhancement can be decomposed using a Raman bond model into contributions from within the molecule, within the metal cluster, and from interfragment interactions. 13 The enhancement also depends on the tip shape and size, ¹⁹ and changes to the molecular structure that tune the tip-molecule chemical interaction also tune the enhancement.^{20,21} However, fully QM studies of TERS images are challenging because of the large number of Raman calculations that must be performed to obtain an image. In several systems of single-atom Ag tips interacting with π -conjugated molecules, DFT-based modeling has shown that the Raman intensity depends strongly on the Angstrom-scale tip position, ^{22,23} the energy of light, 22 and the charge of the tip. 24 Replacing the Ag atom tip with a tetrahedral Ag₂₀ cluster enhances the Raman intensity of different modes to varying extents, changing the observed TERS spectrum.²³ More detailed study is needed to understand the chemical origins of these changes.

We have parametrized the semiempirical INDO model to yield accurate excited-state properties for Ag nanoclusters at the configuration interaction singles (CIS) level. 12,25 Using an INDO-based approach, it is straightforward to decompose the SERS enhancement into EM and CM components at each wavelength. 12 In this decomposition, the SERS spectrum is computed using both the standard INDO/CIS method and a variant called INDO-EM/CIS, where terms in the Hamiltonian related to the overlap of atomic orbitals on the molecule with those on the tip are set to zero, resulting in only EM enhancement. 12 Both the EM and CM enhancements vary substantially with the energy of the incoming light, highlighting the importance of directly modeling QM effects. 12 This approach has also revealed that, in a TERS-like setup, the bias dependence of the enhancement factor results from changes in the energies of charge-transfer excited states.²⁶

Here, we investigate the role of CM enhancement in the TERS images of the prototypical tip—molecule systems Ag_n — CO_2 . When only the EM is present, both the Raman-active and Raman-inactive stretching modes of CO_2 are enhanced by interactions with the tip, and the enhancement decays monotonically as the molecule is moved away from the tip. In contrast, when the CM is also modeled, the two modes have quite distinct spatial patterns of enhancement, including some regions of space where the chemical and electromagnetic enhancements interact constructively and some where they interact destructively. These patterns are largely maintained as the tip length increases. This shows that chemical enhancement is capable of playing a significant role in the spatial enhancement patterns.

2. COMPUTATIONAL METHODS

The geometries of the isolated Ag_n nanowires, the isolated CO_2 molecule, and the Ag_n - CO_2 complexes were optimized using the BP86 functional and the aug-cc-pVDZ basis set for C and O combined with the aug-cc-pVDZ-PP basis set for Ag^{29} using the Gaussian 16 software package.

To generate the TERS images, the geometries of the isolated Ag_n nanowire and CO_2 molecule were placed with their long axes parallel, and at a set displacement distance along both the axis parallel to the molecular long axes (the longitudinal axis) and the axis perpendicular to the molecular long axes (the transverse axis) as shown in Figure 1. The origin (displacement

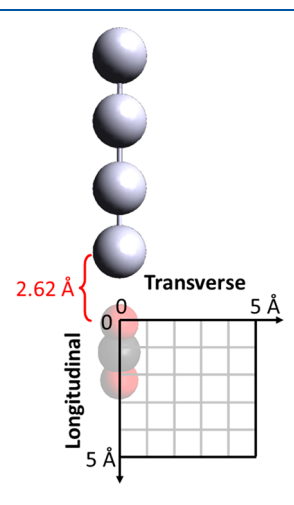


Figure 1. Schematic of the geometries of the Ag_n – CO_2 complex used to generate TERS images.

of zero) was defined by setting the Ag_n-CO₂ distance equal to the distance between the two moieties in the optimized geometry of the complex; this distance is 2.62, 2.61, 2.60, and 2.60 Å for Ag₄, Ag₆, Ag₈, and Ag₁₀, respectively. For each geometry, the Raman intensities were computed using the Intermediate Neglect of Differential Overlap (INDO) Hamiltonian using a sum-over-states (SOS) technique, computing the excited states using a configuration interaction approach with single excitations (CIS). We have previously parametrized INDO for Ag, 12,25 and our approach to computing the Raman intensities is the same as in our previous work. 12,26 Although the calculations do not explicitly include relativistic corrections, our parametrization was performed relative to excited-state energies calculated with zeroth-order relativistic corrections, and thus relativistic effects are implicitly included in our choice of parameters. The Raman intensities were also computed using the modified INDO-EM Hamiltonian, which neglects the CM by setting terms in the Hamiltonian related to the overlap of Ag atomic orbitals with atomic orbitals on any other atom to zero. To obtain smoother evolution of the TERS intensities with position, the SCF convergence criteria were tightened by a factor of 10^{-6} relative to the default values. For all systems, all possible CIS excited states within the INDO basis were computed and included in the SOS procedure. Raman intensities were computed at energies on resonance with the first excited state of the isolated Ag_n nanowires. These resonances occurred at energies of 2.05, 1.60, 1.35, and 1.15 eV for Ag₄, Ag₆, Ag₈, and Ag₁₀, respectively. All INDO-based calculations were performed using MOPAC2016.31,32

3. RESULTS AND DISCUSSION

Here, we investigate the extent to which QM effects influence TERS images via the chemical enhancement mechanism (CM). We focus on the prototypical system of linear Ag_n nanowire tips interacting with the CO_2 molecule. Ag_n nanowires have been widely used as prototypical systems for studies of plasmonics-

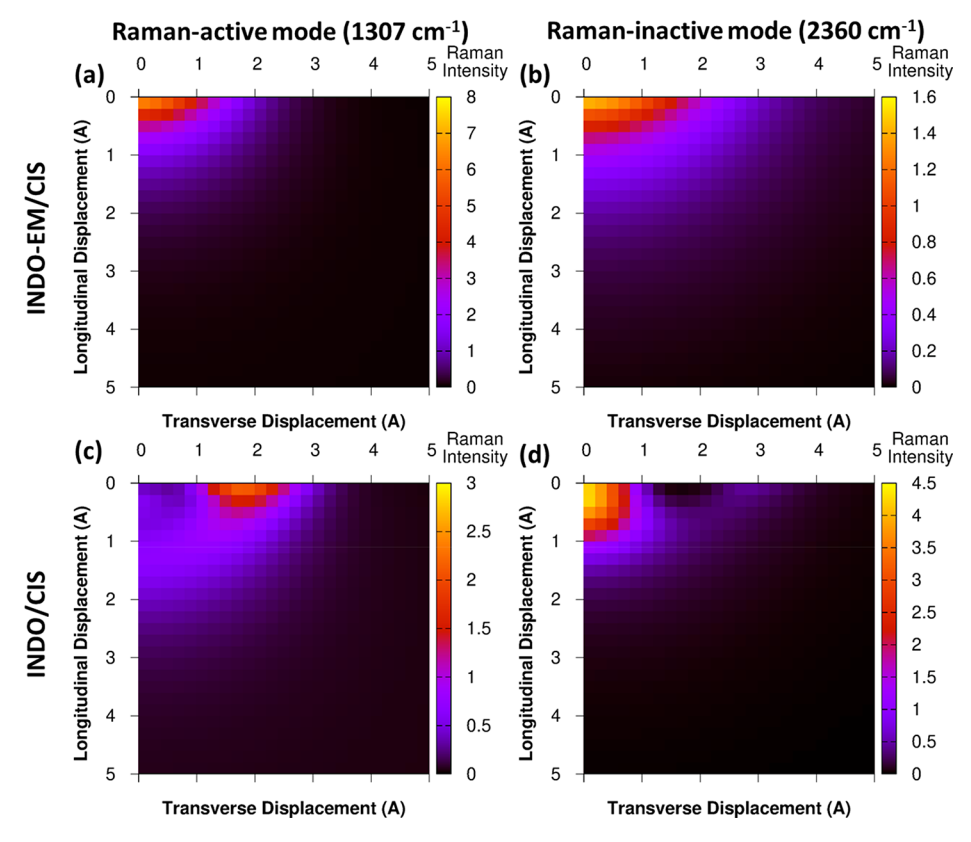


Figure 2. Maps of TERS intensities of the Ag_4 – CO_2 complex as a function of displacement, for the (a,c) Raman-active and (b,d) Raman-inactive stretching modes at the (a,b) INDO-EM/CIS and (c,d) INDO/CIS levels of theory. TERS intensities were computed on resonance with the Ag_4 absorption peak at 2.05 eV.

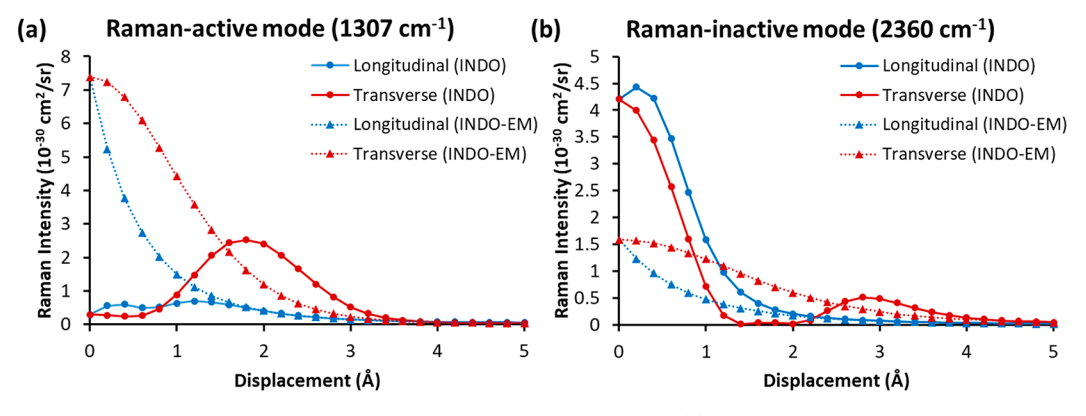


Figure 3. TERS intensities of the Ag₄–CO₂ complex as a function of displacement, for the (a) Raman-active and (b) Raman-inactive stretching modes at the INDO/CIS and INDO-EM/CIS levels of theory. TERS intensities were computed on resonance with the Ag₄ absorption peak at 2.05 eV.

related properties. $^{33-38}$ The nanowires have a strong longitudinal absorption peak that decreases in energy with increasing length, 33,34 allowing us to readily study size dependence. CO_2 was selected because it has both a Raman-active symmetric stretching mode ($1307~\rm cm^{-1}$ at the BP86/cc-pVDZ level) and a Raman-inactive asymmetric stretching mode ($2359~\rm cm^{-1}$). Since near-field effects can make Raman-inactive modes appear in the TERS spectrum, we study both the Raman-active and Raman-inactive modes; the bending modes are not considered here. The geometries used to study this system are laid out in Figure 1. The CO_2 molecule was aligned parallel to the nanowire long axis. Although many experimental TERS imaging studies have been performed using planar molecules that are physisorbed on a substrate (and thus are perpendicular to axis of the TERS tip), this parallel orientation mimics the orientation

of molecules like CO that chemisorb on a substrate.³⁹ The origin, with longitudinal and transverse displacements both equal to zero, is defined as the geometry with the Ag_n – CO_2 distance equal to that in the optimized geometry of the complex. Since these geometries are far from equilibrium, we use the vibrational modes of the isolated CO_2 molecule and thus do not capture any effect of the interaction on the vibrational frequencies.

3.1. Ag₄–CO₂ TERS Images. We focus first on the linear Ag₄ tip and compute the TERS intensities using two approaches: (1) INDO/CIS, which includes both chemical (CM) and electromagnetic (EM) enhancements, and (2) INDO-EM/CIS, which includes only EM enhancements. For the Raman-active vibrational mode (1307 cm⁻¹), the TERS intensity at the INDO-EM/CIS level follows the general pattern expected for

the EM (Figure 2a): the TERS intensity is largest at the origin and decays monotonically as the distance increases in either a longitudinal or transverse direction. The enhancement factor (EF) at the origin is 192, computed based on the Raman intensity of 0.0384 for $\rm CO_2$ at 2.05 eV. As shown in Figure 3a, displacement along a longitudinal direction follows an exponential-like decay of the TERS intensity, whereas transverse displacement yields a Gaussian-like decay over a broader range of distances. This is unsurprising because the actual distance between the nearest atoms of the $\rm CO_2$ molecule and the $\rm Ag_4$ tip increases more quickly for longitudinal displacement than for transverse displacement.

When the full INDO Hamiltonian is used, the spatial pattern of TERS enhancement is much more complex, showing that CM contributions substantially modify the overall EF (Figure 2c). At the origin, the INDO EF for the Raman-active mode is 7.80, a factor of 25 smaller than that for INDO-EM, implying a CM enhancement factor of 0.04 (an enhancement factor <1 indicates suppression of the TERS intensity). Although the CM is generally thought to enhance the TERS signal, chemical effects in this case suppress the TERS signal; we have previously seen suppression to a lesser extent in the Ag₂₀—pyridine complex. ¹² In Ag_4 - CO_2 , the only region of space where the CM increases the TERS intensity is at moderate transverse displacements (1.6– 3.4 Å). At large displacements, the INDO and INDO-EM TERS intensities converge; this convergence occurs at a distance of around 2.0 Å for longitudinal displacements and 3.8 Å for transverse displacements (Figure 3a).

For the Raman-inactive mode (2360 cm⁻¹), the INDO-EM TERS intensity is similarly largest when CO₂ is closest to the Ag₄ tip (Figure 2b). Since this mode is Raman-inactive, the enhancement factor is undefined and any nonzero Raman intensity is due to symmetry-breaking of the system. The peak TERS intensity of this mode is a factor of 4.7 smaller than that of the Raman-active mode, and the TERS intensity decays more slowly with distance than for the Raman-active mode. Calculations using the full INDO Hamiltonian show that the CM substantially modifies the TERS intensity (Figure 2d). In contrast with the Raman-active mode, the CM enhances rather than suppresses the TERS intensity in most positions (Figure 3b). At the origin, the CM enhancement is a factor of 2.6, and the nominally Raman-inactive mode has an intensity 14 times larger than that of the Raman-active mode. This is consistent with previous work showing that short-range effects substantially modify the Raman selection rules.⁶ The only region of space where the CM suppresses the TERS intensity is at moderate transverse displacements (1.0-2.4 Å). Similar to the Ramanactive mode, the INDO and INDO-EM TERS intensities converge to the same values at longitudinal displacements around 2.0 Å and transverse displacements around 4.0 Å.

Understanding the origins of these TERS images requires examining the factors that contribute to the Raman intensity. The Raman intensity is proportional to the square of the derivative of the polarizability with respect to displacement along a vibrational mode. In this complex, the dominant contribution to the polarizability is α_{zz} , where z is the axis parallel to the Ag₄ nanowire long axis. The polarizability is computed within the sum-over-states (SOS) model as

$$\alpha_{zz} = \sum_{e} \frac{\mu_{ge,z}^2}{E_{ge} - \hbar\omega - i\Gamma_{ge}} + \frac{\mu_{ge,z}^2}{E_{ge} + \hbar\omega + i\Gamma_{ge}}$$

where $\mu_{ge,z}$ is the transition dipole moment between the ground state g and excited state e along the z axis, E_{ge} is the energy difference between states g and e, ω is the frequency of light, and Γ_{ge} is a broadening factor set to 0.004 au. When $\hbar\omega$ is resonant with the first excited-state energy, only the resonant excited state has a significant contribution to α_{zz} . Though we compute the orientationally averaged Raman intensity, the contribution of α_{zz} to the Raman intensity is 4-5 orders of magnitude larger than the contribution of any other directional component of the polarizability at this energy. A large Raman cross section for a normal mode results from a large derivative of the first excitedstate properties with respect to displacement *p* along that mode; since the denominator of the first term in α_{zz} is close to zero for the resonant excited state, a large $\frac{dE_{ge}}{dp}$ is essential to obtaining a large Raman cross section. In principle, a large Raman cross section may also result from a large $\frac{d\mu_{ge,z}}{dn}$; however, in practice

 $\mu_{ge,z}$ is much less sensitive to geometric changes than E_{ge} . Although all excited states within the INDO/CIS basis are included in the SOS calculation, test calculations including only the first excited state in the SOS calculation yield TERS intensities within 10–25% of the values from the full SOS calculations. This indicates that the first excited state is the

dominant contributor to the TERS intensity.

The first excited state is essentially a HOMO \rightarrow LUMO transition within the Ag₄ moiety, where both HOMO and LUMO are σ -type MOs composed largely of Ag 5s atomic orbitals (AOs). We examine two major factors that contribute to changes in the first excited-state energy E_{ge} of the Ag₄–CO₂ complex, focusing on the complex where CO₂ is at the origin: (1) the extent of ground-state CT from CO₂ to Ag₄ and (2) the effective electric field across the Ag₄ moiety. To understand the effects of ground-state CT, we articificially increase or decrease the Ag AO energies by a small amount (Figure 4). When using

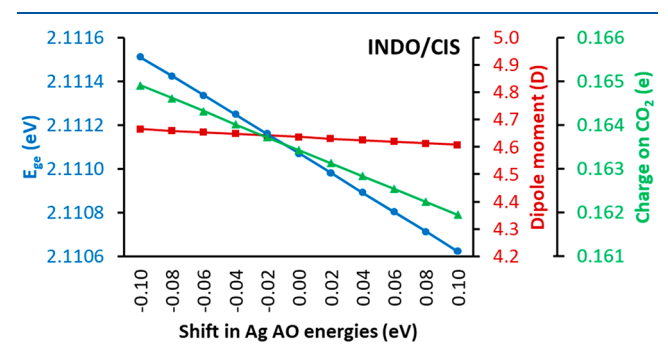


Figure 4. Dependence of the excited-state energy, ground-state dipole moment, and ground-state charge on CO_2 on the Ag atomic orbital energies for the Ag_4 – CO_2 complex at the INDO/CIS level of theory.

the default Ag AO energies, 0.163 e is transferred from CO₂ to Ag₄ in the ground state, resulting in a dipole moment of 4.64 D. An increase in the Ag AO energies drives electrons from Ag₄ to CO₂, decreasing the charge on CO₂ and slightly decreasing the dipole moment of the system. As the Ag AO energies increase, the HOMO is destabilized slightly more than the LUMO, so E_{ge}

A second factor that can affect E_{gc} is the effective electric field across the Ag₄ moiety, which we model by applying a uniform electric field along the long axis of the system. When a positive field is applied, the dipole moment and the charge on the CO₂ moiety both decrease (Figure 5a), similar to the AO energy

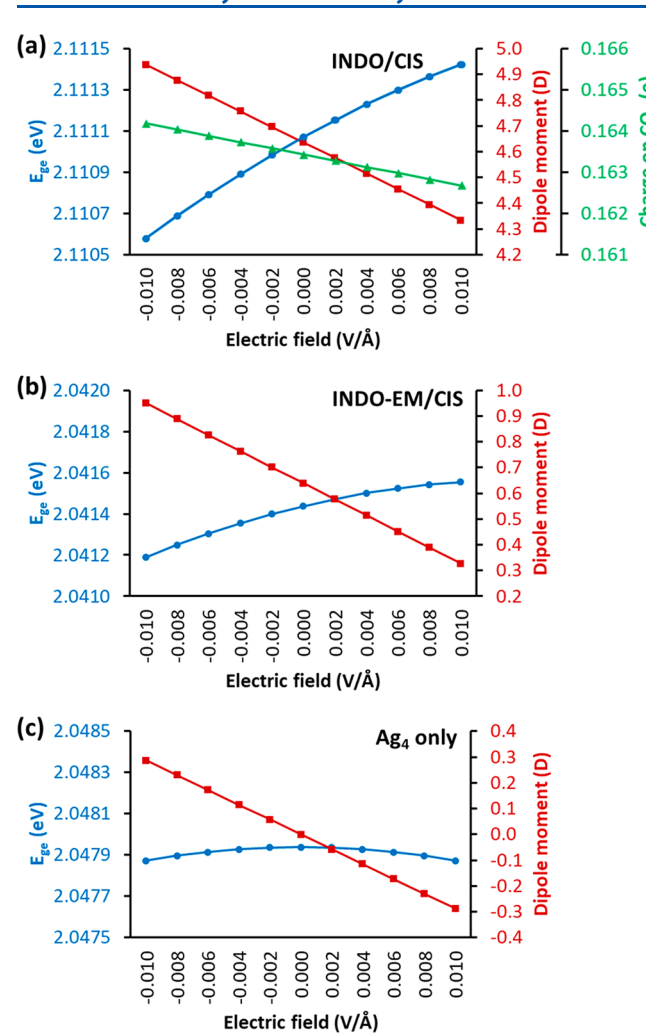


Figure 5. Dependence of the excited-state energy, ground-state dipole moment, and ground-state charge on CO_2 on the applied electric field for (a) the Ag_4 – CO_2 complex at the INDO/CIS level, (b) the Ag_4 – CO_2 complex at the INDO-EM/CIS level, and (c) the isolated Ag_4 cluster at the INDO/CIS level.

shifts; however, the relative magnitudes of the changes to the dipole moment and the charge are quite different. In the first case, the AO shift necessary to increase the charge on CO₂ by 0.01 e increases the dipole moment by 0.194 D; when an electric field is applied, the field that increases the charge on CO₂ by the same amount increases the dipole moment by 3.99 D, a factor of 20.5 larger. When the change in electronic structure is dominated by changes in the dipole moment, the effects are quite distinct from the changes caused by CT. With no applied electric field, the electric field of the CO2 molecule has a symmetry-breaking effect on Ag₄, redistributing both the HOMO and the LUMO toward the end of Ag₄ farthest from the CO₂ molecule; this redistribution decreases the HOMO-LUMO gap and E_{ge} . When a positive electric field is applied, the HOMO and LUMO become more symmetrically distributed, increasing E_{ge} . This means that E_{ge} is anticorrelated with both the dipole moment and the charge on CO2, which is the reverse of the trend observed for shifts in the AO energies.

The change in E_{ge} with electric field can be understood by comparing the INDO/CIS results for the Ag_4 – CO_2 complex to the analogous results for the isolated Ag_4 nanowire (Figure 5c) and for the Ag_4 – CO_2 complex at the INDO-EM/CIS level

(Figure 5b). In all three cases, the change in the dipole moment with electric field is quite similar. Since the isolated Ag₄ nanowire is symmetric, positive and negative fields both break the symmetry and decrease E_{ge} , showing that symmetry-breaking due to the presence of the $\rm CO_2$ molecule is necessary to create a nonzero slope of E_{ge} at the zero-field limit. For the Ag₄–CO₂ complex at the INDO-EM/CIS level, ground-state CT is forbidden, which means that the HOMO and LUMO are more symmetric than at the INDO/CIS level. The slope of E_{ge} is 40% of its value at the INDO/CIS level, which is consistent with a degree of symmetry-breaking that is intermediate between that of the other two systems. This suggests that chemical effects in the form of ground-state CT enhance the dependence of E_{ge} on the electric field.

These model systems provide a framework to understand the spatial patterns in the TERS images. For the Raman-active mode within the INDO-EM model, as both C=O bonds are stretched (defined as positive displacement), E_{ge} decreases, indicating that the derivative $\frac{\mathrm{d}E_{ge}}{\mathrm{d}p}$ is negative (Figure 6a). As the distance between the two moieties increases, $\frac{\mathrm{d}E_{ge}}{\mathrm{d}p}$ approaches zero monotonically, and the shapes of the curves of $\frac{\mathrm{d}E_{ge}}{\mathrm{d}p}$ for longitudinal and transverse displacement strongly resemble the shapes of the curves for the TERS intensity for the same displacements, shown in Figure 3a. Since no ground-state CT is possible within this model, the only mechanism by which CO_2 can induce changes in the Ag_4 moiety is via its electric field, which decays with increasing distance.

When we consider the full INDO Hamiltonian, ground-state CT from CO2 to Ag4 significantly modifies the excited-state properties. The derivative of the charge on CO₂ with respect to displacement $\frac{dq_{\omega_2}}{dp}$ is positive, indicating that stretching of the C=O bonds and shortening the Ag···O distance results in more CT from CO₂ to Ag₄ (Figure 6c). $\frac{dq_{co2}}{dp}$ is largest in magnitude at longitudinal and transverse displacements of 0.2 and 1.0 Å and decays to zero at longitudinal and transverse displacements around 2.2 and 4.0 Å, respectively. This chemical interaction between the Ag₄ and CO₂ moieties significantly changes $\frac{dE_g}{dp}$. When CO₂ is close to Ag₄, the EM and CM effects counteract each other: the EM has a negative contribution to $\frac{dE_{ge}}{dp}$, whereas the CM has a positive contribution. At the shortest displacements, the CM slightly outweighs the EM, leading to a small positive $\frac{dE_{gr}}{dp}$. This is consistent with the very small TERS intensity in this distance range. The positive sign of the CM contributions, implying that an increase positive charge on $\ensuremath{\text{CO}}_2$ causes an increase in E_{ge} , suggest that the CM for this mode is driven primarily by changes in ground-state CT and not by changes in the electric field. This is unsurprising because symmetric stretching of the isolated CO₂ molecule results in no net dipole moment, so the changes in electric field should be small.

As displacement increases in the longitudinal direction, $\frac{dE_g}{dp}$ converges to its value within the INDO-EM model around 2.0 Å, approximately the same distance at which the INDO and INDO-EM TERS intensities converge. In contrast, displacements in the transverse direction show more complex behavior. The INDO/

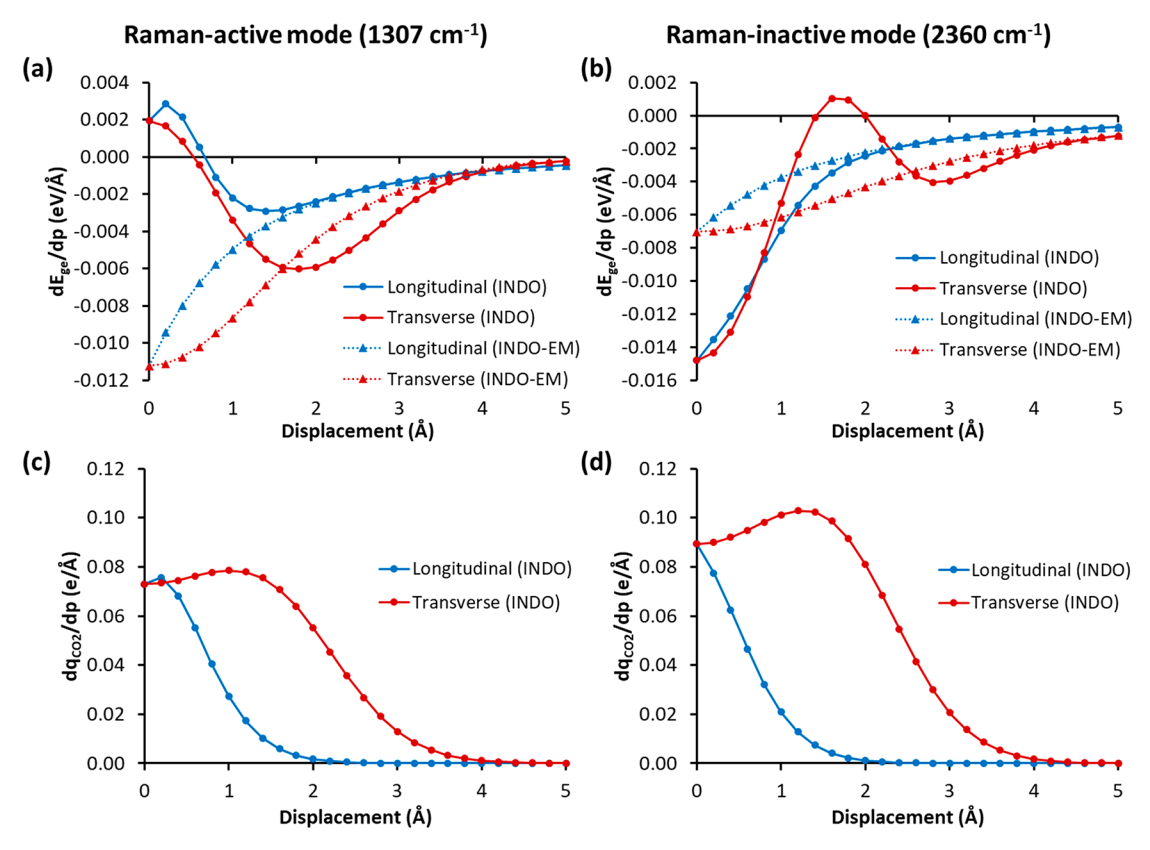


Figure 6. Derivative of the (a, b) excited-state energy and (c, d) ground-state charge on CO₂ with respect to displacement along the (a, c) Ramanactive and (b, d) Raman-inactive modes for the Ag₄–CO₂ complex at the INDO/CIS and INDO-EM/CIS levels of theory.

CIS $\frac{dE_{ge}}{dp}$ values are larger in magnitude than the corresponding INDO-EM/CIS values from 1.8 to 3.8 Å, the same distance range at which the INDO TERS intensity is larger than the INDO-EM intensity. The reversal in the sign of the CM is due to changes in the selection rules for orbital mixing for transverse displacements. At a transverse displacement of zero, the long axes of Ag₄ and CO₂ are perfectly aligned, so MOs on one moiety with σ -type character can only mix with σ -type MOs on the other moiety, and likewise for π -type MOs. The first excited state is essentially a HOMO → LUMO transition, where both HOMO and LUMO are σ -type MOs primarily on the Ag₄ moiety. At moderate transverse displacements, the first excited state acquires small contributions from excitations from the HOMO on Ag₄ into a π^* MO on CO₂, resulting in a negative peak in $\frac{dE_{ge}}{dp}$ at moderate transverse displacements. At large transverse displacements, the AO overlaps are small enough that the $\sigma \to \pi^*$ contributions to the first excited state are negligibly small, and $\frac{\mathrm{d} E_{ge}}{\mathrm{d} p}$ approaches its INDO-EM value.

For the Raman-inactive mode, $\frac{dE_{ge}}{dp}$ likewise strongly correlates with the TERS intensity. A positive displacement along the vibrational mode is defined as stretching the C=O bond closer to the Ag₄ nanowire and compressing the C=O bond farther from the nanowire. At the INDO-EM level, $\frac{dE_{ge}}{dp}$ is negative for all geometries. At the origin, $\frac{dE_{ge}}{dp}$ for the Raman-inactive mode is around 60% of the corresponding value for the Raman-active mode (Figure 6b). This largely accounts for the lower TERS

intensity of the Raman-inactive mode. As the distance increases in either a longitudinal or transverse direction, $\frac{dE_{gc}}{dp}$ decreases monotonically.

At the INDO level, chemical effects substantially modify $\frac{dE_{ge}}{dn}$. Similar to the case of the Raman-active mode, $\frac{dq_{co2}}{dp}$ is positive at small displacements, corresponding to more ground-state CT from CO₂ to Ag₄ as the Ag···O distance decreases (Figure 6d). However, unlike for the Raman-active mode, both the EM and CM have negative contributions to $\frac{\mathrm{d}E_{\mathrm{ge}}}{\mathrm{d}p}$ at small displacements. This is due to a reversal in the relative significance of electric field vs CT effects. Displacement of CO₂ along the Raman-inactive mode causes large changes to its dipole moment and thus to the electric field experienced by the Ag₄ moiety. Since electric field contributions have the opposite sign contribution to $\frac{dE_{ge}}{dp}$ as CT effects, the dominance of electric field contributions accounts for the opposite sign of the CM contribution to $\frac{\mathrm{d}E_{ge}}{\mathrm{d}p}$ relative to the Raman-active mode. The mutual enhancement of the EM and CM contributions cause the Raman-inactive mode to have larger $\frac{dE_{ge}}{\cdot}$ and TERS intensity than the Raman-active mode at small displacements, reversing the selection rules for the isolated CO2 molecule.

As the displacement increases in the longitudinal direction, $\frac{\mathrm{d}E_{ge}}{\mathrm{d}p}$ for the Raman-inactive mode within the INDO model smoothly approaches its value within the INDO-EM model, and the two models yield nearly identical results at displacements

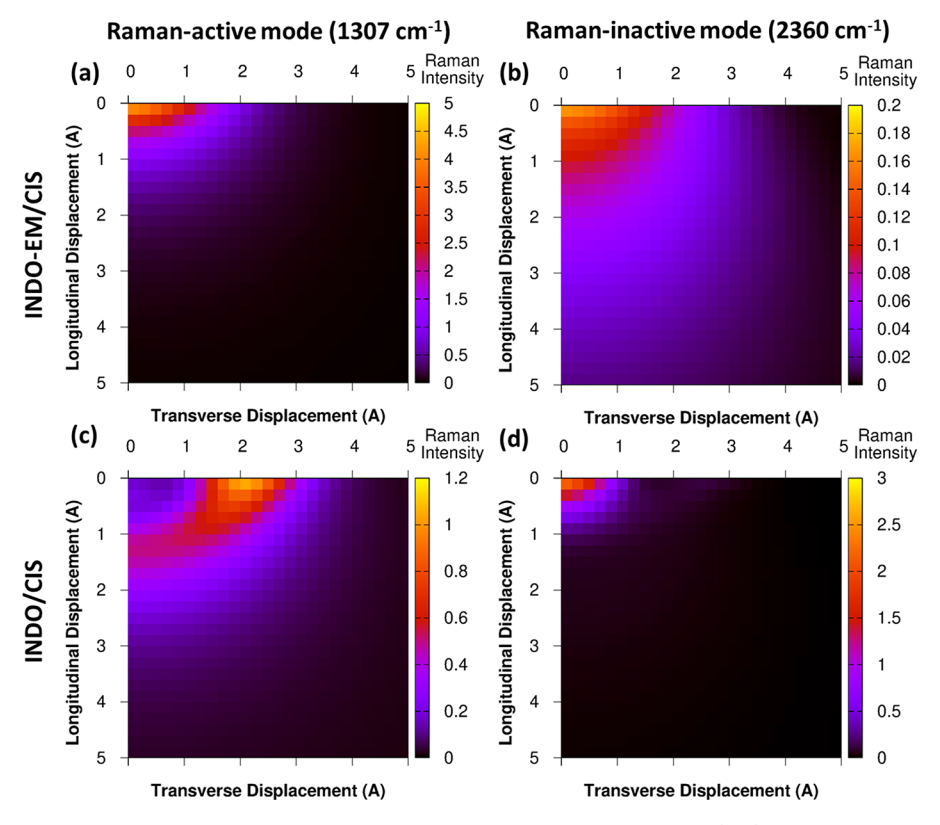


Figure 7. Maps of TERS intensities of the Ag_6 – CO_2 complex as a function of displacement, for the (a, c) Raman-active and (b, d) Raman-inactive stretching modes at the (a, b) INDO-EM/CIS and (c, d) INDO/CIS levels of theory. TERS intensities were computed on resonance with the Ag_6 absorption peak at 1.60 eV.

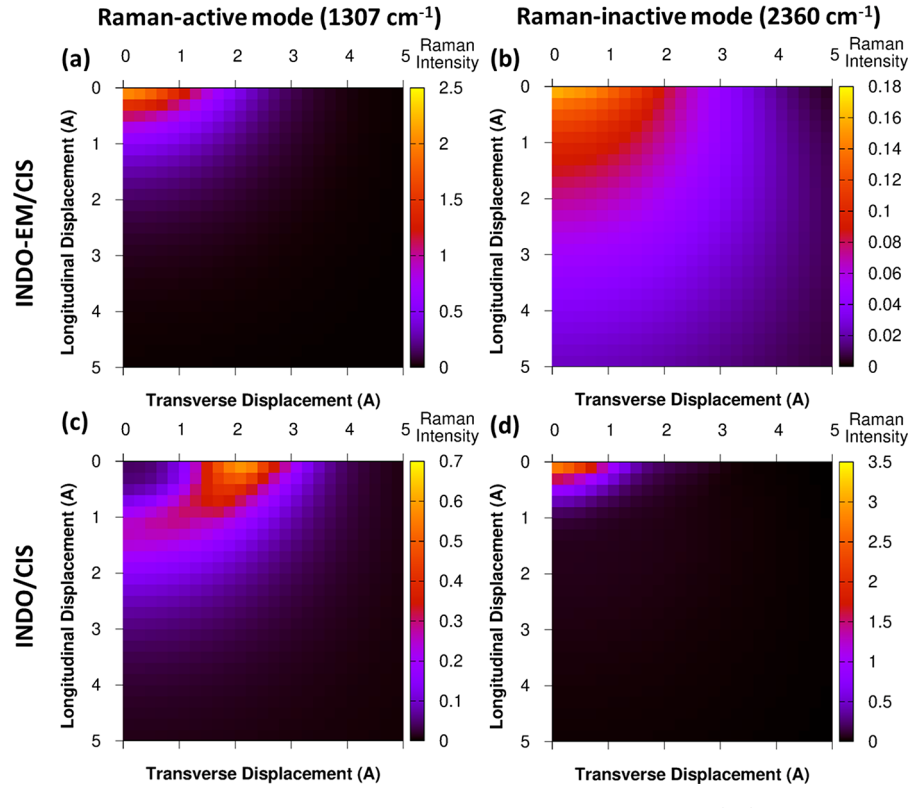


Figure 8. Maps of TERS intensities of the Ag_8 – CO_2 complex as a function of displacement, for the (a,c) Raman-active and (b,d) Raman-inactive stretching modes at the (a,b) INDO-EM/CIS and (c,d) INDO/CIS levels of theory. TERS intensities were computed on resonance with the Ag_8 absorption peak at 1.35 eV.

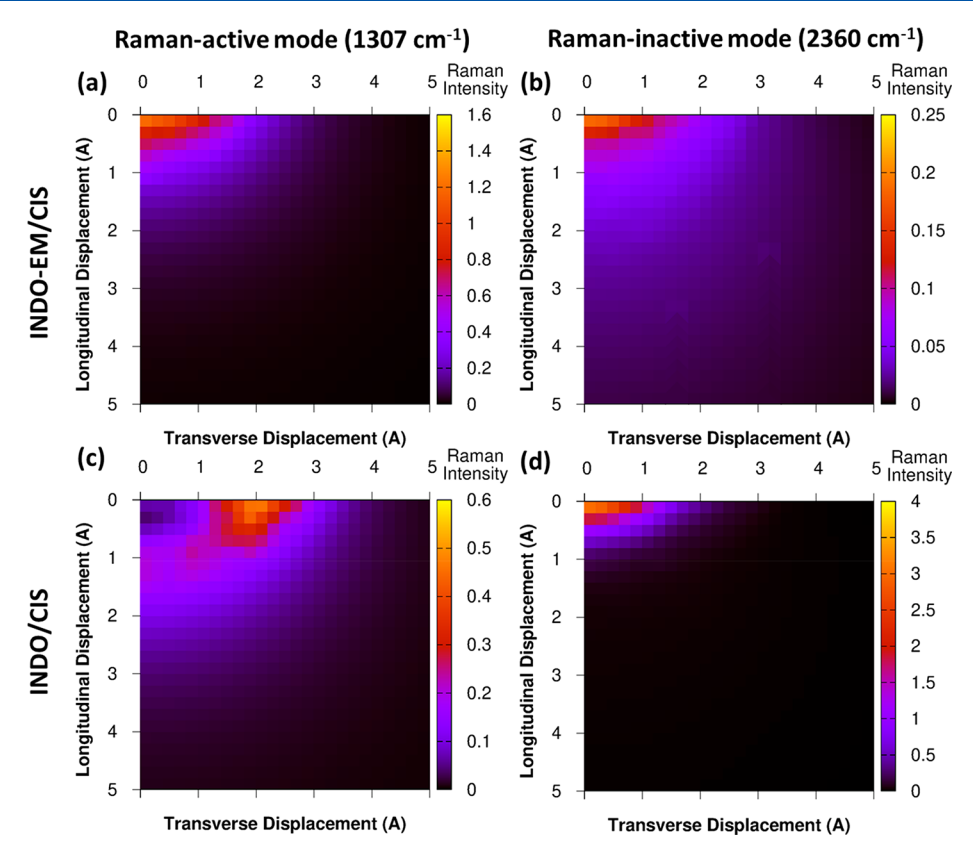


Figure 9. Maps of TERS intensities of the Ag_{10} – CO_2 complex as a function of displacement, for the (a, c) Raman-active and (b, d) Raman-inactive stretching modes at the (a, b) INDO-EM/CIS and (c, d) INDO/CIS levels of theory. TERS intensities were computed on resonance with the Ag_{10} absorption peak at 1.15 eV.

larger than 2.0 Å. This trend is similar to that seen for the Raman-active mode. In contrast, the magnitude of $\frac{dE_{ge}}{dn}$ is smaller

for INDO than for INDO-EM for transverse displacements between 1.0 and 2.4 Å, accounting for the suppression of the TERS intensity at moderate transverse displacements. Similar to the Raman-active mode, this suppression of the TERS intensity is related to mixing of small amounts of $\sigma \to \pi^*$ character into the first excited state.

3.2. Effect of Ag_n Length on TERS Images. We now examine the effect of the Ag_n nanowire length on the TERS images, comparing our n = 4 results from the previous section (Figure 2) to nanowires with n = 6 (Figure 7), n = 8 (Figure 8), and n = 10 (Figure 9). The overall features of the TERS images are consistent across the series of nanowire lengths. In the INDO-EM maps, the TERS intensity is largest when the CO₂ molecule is closest to the Ag_n tip and decays monotonically as distance increases; this decay is exponential-like for longitudinal displacements and Gaussian-like for transverse displacements (Figure 10). For the Ag_{10} – CO_2 complex, there is noticeable noise in the TERS intensities because of the challenges of obtaining converged properties within a SOS approach for systems with thousands of excited states. For the Raman-active mode, the TERS EF when CO₂ is at the origin increases with increasing nanowire length: the EF is 192, 381, 420, and 545 for the Ag₄, Ag₆, Ag₈, and Ag₁₀ nanowires, respectively. The increase in EF is not apparent when looking at the raw TERS intensities because all TERS intensities are computed on resonance with the nanowire first excited state, which decreases in energy with increasing length. The Raman intensity of the isolated CO₂ molecule decreases with decreasing energy. The relative TERS

intensities of the Raman-active and Raman-inactive modes show less consistent trends with nanowire length: the Raman-active mode has a larger TERS intensity by a factor of 4.7, 26, 14, and 6.9, respectively, for the Ag₄, Ag₆, Ag₈, and Ag₁₀ nanowires. As discussed previously, the EFs for the Raman-inactive mode cannot be defined.

Within the INDO model, chemical effects substantially modify the TERS images. For the Raman-active mode, all four nanowires have qualitatively similar TERS profiles, with the exception of the noise in the case of Ag₁₀. For all nanowire lengths, chemical effects suppress the TERS intensity of the Raman-active mode by more than an order of magnitude at small displacements; when CO₂ is at the origin, the EF at the INDO level is 7.8, 11, 7.2, and 22 for the Ag₄, Ag₆, Ag₈, and Ag₁₀ nanowires, respectively. This shows that cancellation between EM and CM effects is present across this full series of nanowires. For all four nanowires, displacement along the Raman-active mode primarily changes the ground-state CT but has minimal effects on the dipole moment, meaning that the CM and EM have opposite sign contributions to $\frac{dE_{ge}}{dp}$. The TERS intensity peaks at longitudinal displacements of 1.0-1.2 Å, and the INDO and INDO-EM TERS intensities converge at displacements around 2.0 Å. For transverse displacements, the INDO TERS intensity is consistently larger than the INDO-EM TERS intensity at moderate displacements where mixing between σ type and π -type orbitals is largest. The TERS intensity peaks at a transverse displacement of 1.8 Å for Ag₄ and 2.2 Å for the longer three nanowires.

For the Raman-inactive mode, chemical effects consistently lead to strong enhancement of the TERS intensity at small

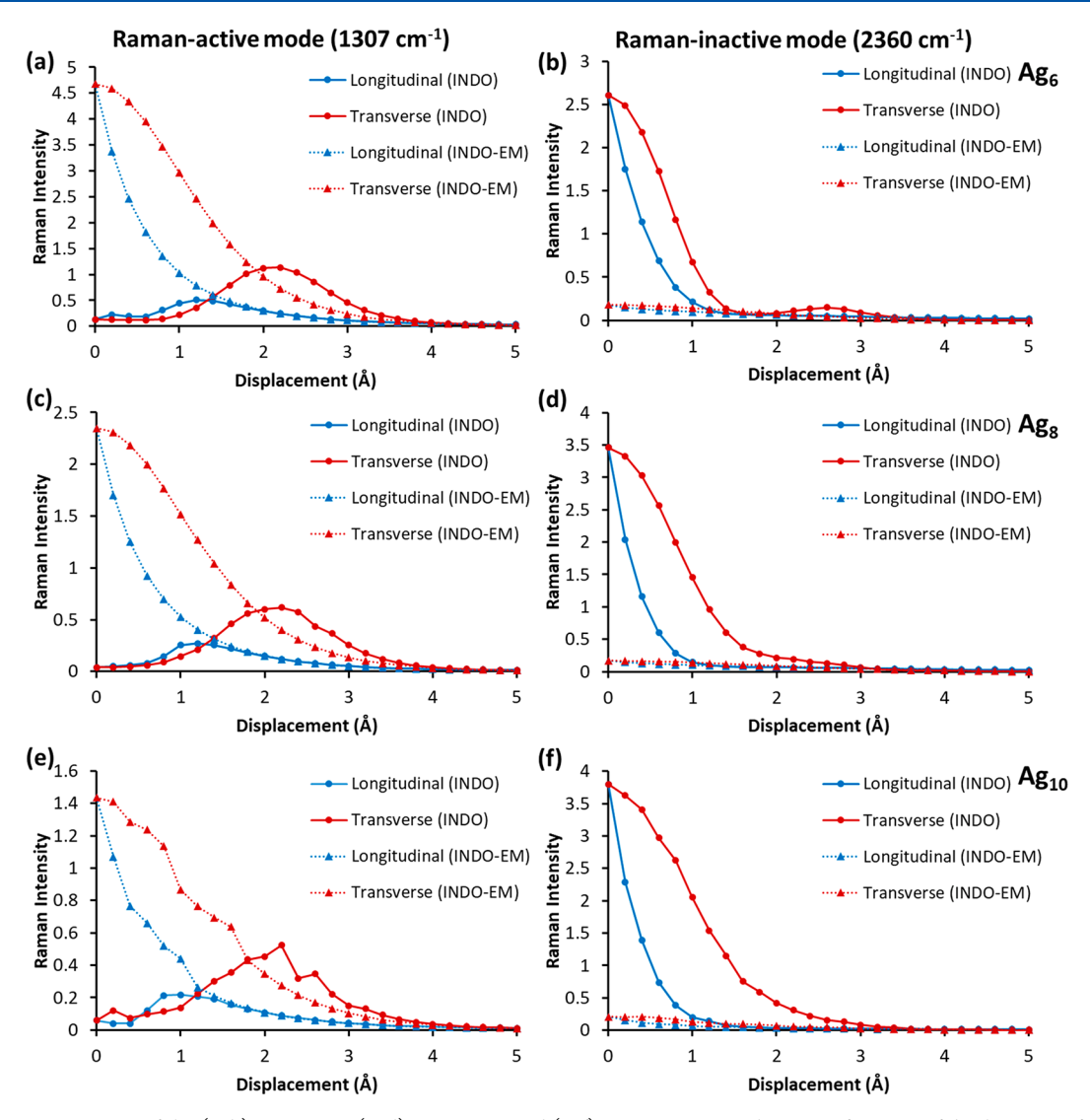


Figure 10. TERS intensities of the (a, b) Ag_6-CO_2 , (c, d) Ag_8-CO_2 , and (e, f) $Ag_{10}-CO_2$ complexes as a function of displacement, for the (a, c, e) Raman-active and (b, d, f) Raman-inactive stretching modes at the INDO/CIS and INDO-EM/CIS levels of theory.

displacements. For Ag₄, chemical effects cause the INDO TERS intensity to be a factor of 2.6 larger than the INDO-EM intensity at the origin. The chemical effect is much larger for the longer nanowires: a factor of 14, 20, and 18, respectively for the Ag₆, Ag₈, and Ag₁₀ nanowires. This enhancement is due to the electric field produced by CO₂. For longitudinal displacements, the TERS intensity decays monotonically, and the INDO and INDO-EM intensities converge around 1.8 Å. However, for transverse displacements, the profile of the TERS intensity changes with nanowire length. For Ag4, there is a prominent suppression of the TERS intensity at transverse displacements of 1.0–2.6 Å due to mixing between σ -type and π -type orbitals. As the nanowire length increases, this suppression disappears: Ag₆ has a small suppression of the TERS intensity at transverse displacements of 1.4–2.4 Å, and no suppression is observable for Ag₈ and Ag₁₀. This suggests that different aspects of the CM have different dependence on the nanowire length.

4. CONCLUSIONS

Understanding the enhancement mechanisms contributing to the TERS intensity at short ranges is essential to interpreting TERS images on the subnm scale. Using a model system of CO₂

interacting with Ag_n tips, we have shown that chemical enhancement effects play a substantial role in determining the intensity of the TERS signal at short interaction distances. These chemical effects are captured by choosing a level of theory that enables us to treat the full molecule—tip complex quantum mechanically. When the tip and molecule are nearly touching, these chemical effects are large enough that the nominally Raman-inactive mode of CO_2 has a larger TERS intensity than the nominally Raman-active mode. The chemical effects become negligibly small at distances of more than a few angstroms.

Even in such a small model system, there are at least three distinct mechanisms by which chemical effects modify the TERS intensity, all of which affect how sensitive the first excited-state energy is to changes in the molecular geometry:

- 1. Fluctuations in the effective electric field of the molecule. This effect is particularly prominent for the Ramaninactive mode and interferes constructively with the EM enhancements, leading to strong TERS enhancement.
- 2. Fluctuations in the extent of ground-state CT. This effect is dominant for the Raman-active mode and interferes destructively with the EM enhancements, leading to suppression of the TERS signal.

3. Mixing between σ -type and π -type orbitals. This effect is significant for both vibrational modes at moderate transverse displacements. The mixing leads to enhancement of the TERS signal for the Raman-active mode and suppression for the Raman-inactive mode. For the Raman-inactive mode, this effect becomes less significant with increasing tip length.

This wide variety of chemical effects suggests that chemical contributions to TERS images are not only significant contributors to the TERS intensity but also strongly system-dependent and mode-dependent. Detailed study of additional systems is needed to understand the extent to which similar chemical effects are seen in other systems and to extend these results to molecules and tips more similar to those studied experimentally. Further work examining the effects of factors such as the orientation of the molecule and its interaction with a substrate will give insight into how chemical effects modify the TERS images observed experimentally.

ASSOCIATED CONTENT

Solution Supporting Information

The Supporting Information is available free of charge at https://pubs.acs.org/doi/10.1021/acs.jpcc.2c03309.

Optimized coordinates of Ag_n nanowires and Ag_n - CO_2 complexes. (PDF)

AUTHOR INFORMATION

Corresponding Author

Rebecca L. M. Gieseking — Department of Chemistry, Brandeis University, Waltham, Massachusetts 02453, United States; orcid.org/0000-0002-7343-1253; Phone: (781)-736-2511; Email: gieseking@brandeis.edu

Complete contact information is available at: https://pubs.acs.org/10.1021/acs.jpcc.2c03309

Notes

The author declares no competing financial interest.

ACKNOWLEDGMENTS

This project was supported by an NSF CAREER award (CHE-2046099). Computational work was performed on the Brandeis HPCC, which is partially supported by the NSF through DMR-MRSEC 2011846 and OAC-1920147

■ REFERENCES

- (1) Jiang, N.; Kurouski, D.; Pozzi, E. A.; Chiang, N.; Hersam, M. C.; Van Duyne, R. P. Tip-Enhanced Raman Spectroscopy: From Concepts to Practical Applications. *Chem. Phys. Lett.* **2016**, *6*59, 16–24.
- (2) Richard-Lacroix, M.; Zhang, Y.; Dong, Z.; Deckert, V. Mastering High Resolution Tip-Enhanced Raman Spectroscopy: Towards a Shift of Perception. *Chem. Soc. Rev.* **2017**, *46* (13), 3922–3944.
- (3) Langer, J.; Jimenez de Aberasturi, D.; Aizpurua, J.; Alvarez-Puebla, R. A.; Auguié, B.; Baumberg, J. J.; Bazan, G. C.; Bell, S. E. J.; Boisen, A.; Brolo, A. G.; et al. Present and Future of Surface-Enhanced Raman Scattering. ACS Nano 2020, 14 (1), 28–117.
- (4) Zhang, R.; Zhang, Y.; Dong, Z. C.; Jiang, S.; Zhang, C.; Chen, L. G.; Zhang, L.; Liao, Y.; Aizpurua, J.; Luo, Y.; et al. Chemical Mapping of a Single Molecule by Plasmon-Enhanced Raman Scattering. *Nature* **2013**, 498 (7452), 82–86.
- (5) Lee, J.; Crampton, K. T.; Tallarida, N.; Apkarian, V. A. Visualizing Vibrational Normal Modes of a Single Molecule with Atomically Confined Light. *Nature* **2019**, *568* (7750), 78–82.

- (6) Tallarida, N.; Lee, J.; Apkarian, V. A. Tip-Enhanced Raman Spectromicroscopy on the Angstrom Scale: Bare and CO-Terminated Ag Tips. ACS Nano 2017, 11 (11), 11393–11401.
- (7) Nie, S.; Emory, S. R. Probing Single Molecules and Single Nanoparticles by Surface-Enhanced Raman Scattering. *Science.* **1997**, 275, 1102–1107.
- (8) Kneipp, K.; Wang, Y.; Kneipp, H.; Perelman, L. T.; Itzkan, I.; Dasari, R. R.; Feld, M. S. Single Molecule Detection Using Surface-Enhanced Raman (SERS). *Phys. Rev. Lett.* **1997**, *78*, 1667–1670.
- (9) Willets, K. A.; Van Duyne, R. P. Localized Surface Plasmon Resonance Spectroscopy and Sensing. *Annu. Rev. Phys. Chem.* **2007**, *58*, 267–297.
- (10) Xu, H.; Aizpurua, J.; Käll, M.; Apell, P. Electromagnetic Contributions to Single-Molecule Sensitivity in Surface-Enhanced Raman Scattering. *Phys. Rev. E* **2000**, *62* (3), 4318–4324.
- (11) Morton, S. M.; Silverstein, D. W.; Jensen, L. Theoretical Studies of Plasmonics Using Electronic Structure Methods. *Chem. Rev.* **2011**, 111, 3962–3994.
- (12) Gieseking, R. L.; Ratner, M. A.; Schatz, G. C. Theoretical Modeling of Voltage Effects and the Chemical Mechanism in Surface-Enhanced Raman Scattering. *Faraday Discuss.* **2017**, 205, 149–171.
- (13) Chen, R.; Jensen, L. Quantifying the Enhancement Mechanisms of Surface-Enhanced Raman Scattering Using a Raman Bond Model. *J. Chem. Phys.* **2020**, *153* (22), 224704.
- (14) Lee, J.; Tallarida, N.; Chen, X.; Liu, P.; Jensen, L.; Apkarian, V. A. Tip-Enhanced Raman Spectromicroscopy of Co(II)-Tetraphenylporphyrin on Au(111): Toward the Chemists' Microscope. *ACS Nano* **2017**, *11*, 11466–11474.
- (15) Chen, X.; Liu, P.; Hu, Z.; Jensen, L. High-Resolution Tip-Enhanced Raman Scattering Probes Sub-Molecular Density Changes. *Nat. Commun.* **2019**, *10* (1), 2567.
- (16) Liu, P.; Chulhai, D. V.; Jensen, L. Single-Molecule Imaging Using Atomistic Near-Field Tip-Enhanced Raman Spectroscopy. *ACS Nano* **2017**, *11* (5), 5094–5102.
- (17) Liu, P.; Chen, X.; Ye, H.; Jensen, L. Resolving Molecular Structures with High-Resolution Tip-Enhanced Raman Scattering Images. *ACS Nano* **2019**, *13* (8), 9342–9351.
- (18) Zhao, L.; Jensen, L.; Schatz, G. C. Pyridine-Ag20 Cluster: A Model System for Studying Surface-Enhanced Raman Scattering. *J. Am. Chem. Soc.* **2006**, *128*, 2911–2919.
- (19) Jensen, L.; Zhao, L. L.; Schatz, G. C. Size-Dependence of the Enhanced Raman Scattering of Pyridine Adsorbed on Agn (n = 2-8, 20) Clusters. J. Phys. Chem. C 2007, 111, 4756-4764.
- (20) Valley, N.; Greeneltch, N.; Van Duyne, R. P.; Schatz, G. C. A Look at the Origin and Magnitude of the Chemical Contribution to the Enhancement Mechanism of Surface-Enhanced Raman Spectroscopy (SERS): Theory and Experiment. *J. Phys. Chem. Lett.* **2013**, *4*, 2599–2604
- (21) Trivedi, D. J.; Barrow, B.; Schatz, G. C. Understanding the Chemical Contribution to the Enhancement Mechanism in SERS: Connection with Hammett Parameters. *J. Chem. Phys.* **2020**, *153* (12), 124706.
- (22) Fiederling, K.; Abasifard, M.; Richter, M.; Deckert, V.; Gräfe, S.; Kupfer, S. The Chemical Effect Goes Resonant a Full Quantum Mechanical Approach on TERS. *Nanoscale* **2020**, *12* (11), 6346–6359.
- (23) Latorre, F.; Kupfer, S.; Bocklitz, T.; Kinzel, D.; Trautmann, S.; Gräfe, S.; Deckert, V. Spatial Resolution of Tip-Enhanced Raman Spectroscopy-DFT Assessment of the Chemical Effect. *Nanoscale* **2016**, *8* (19), 10229–10239.
- (24) Fiederling, K.; Kupfer, S.; Gräfe, S. Are Charged Tips Driving TERS-Resolution? A Full Quantum Chemical Approach. *J. Chem. Phys.* **2021**, *154* (3), 034106.
- (25) Gieseking, R. L.; Ratner, M. A.; Schatz, G. C. Semiempirical Modeling of Ag Nanoclusters: New Parameters for Optical Property Studies Enable Determination of Double Excitation Contributions to Plasmonic Excitation. *J. Phys. Chem. A* **2016**, *120*, 4542–4549.
- (26) Gieseking, R. L. M.; Lee, J.; Tallarida, N.; Apkarian, V. A.; Schatz, G. C. Bias-Dependent Chemical Enhancement and Nonclassical Stark

Effect in Tip-Enhanced Raman Spectromicroscopy of CO-Terminated Ag Tips. J. Phys. Chem. Lett. 2018, 9, 3074-3080.

- (27) Becke, A. D. Density-Functional Exchange-Energy Approximation with Correct Asymptotic Behavior. Phys. Rev. A 1988, 38, 3098-
- (28) Perdew, J. P. Density-Functional Approximation for the Correlation Energy of the Inhomogeneous Electron Gas. Phys. Rev. B 1986, 33, 8822-8824.
- (29) Dunning, T. H., Jr. Gaussian Basis Sets for Use in Correlated Molecular Calculations. I. The Atoms Boron through Neon and Hydrogen. J. Chem. Phys. 1989, 90, 1007-1023.
- (30) Frisch, M. J.; Trucks, G. W.; Schlegel, H. B.; Scuseria, G. E.; Robb, M. A.; Cheeseman, J. R.; Scalmani, G.; Barone, V.; Petersson, G. A.; Nakatsuji, H.; et al. Gaussian 16, Revision B.01; Gaussian, Inc.: Wallingford, CT, 2016.
- (31) MOPAC2016; Stewart, J. J. P. MOPAC2016. Stewart Computational Chemistry; Colorado Springs, CO, USA.
- (32) Gieseking, R. L. M. A New Release of MOPAC Incorporating the INDO/S Semiempirical Model with CI Excited States. J. Comput. Chem. 2021, 42 (5), 365-378.
- (33) Guidez, E. B.; Aikens, C. M. Theoretical Analysis of the Optical Excitation Spectra of Silver and Gold Nanowires. Nanoscale 2012, 4 (14), 4190.
- (34) Yan, J.; Gao, S. Plasmon Resonances in Linear Atomic Chains: Free-Electron Behavior and Anisotropic Screening of d Electrons. Phys. Rev. B 2008, 78 (23), 235413.
- (35) Gieseking, R. L. M. Third-Order Nonlinear Optical Properties of Ag Nanoclusters: Connecting Molecule-like and Nanoparticle-like Behavior. Chem. Mater. 2019, 31 (17), 6850-6859.
- (36) Pandeya, P.; Aikens, C. M. Theoretical Analysis of Optical Absorption Spectra of Parallel Nanowire Dimers and Dolmen Trimers. J. Phys. Chem. C 2020, 124 (24), 13495-13507.
- (37) Ding, F.; Guidez, E. B.; Aikens, C. M.; Li, X. Quantum Coherent Plasmon in Silver Nanowires: A Real-Time TDDFT Study. J. Chem. Phys. 2014, 140, 244705.
- (38) Bernadotte, S.; Evers, F.; Jacob, C. R. Plasmons in Molecules. J. Phys. Chem. C 2013, 117 (4), 1863–1878.
- (39) Zhang, P.; Chen, Y.-X.; Cai, J.; Liang, S.-Z.; Li, J.-F.; Wang, A.; Ren, B.; Tian, Z.-Q. An Electrochemical in Situ Surface-Enhanced Raman Spectroscopic Study of Carbon Monoxide Chemisorption at a Gold Core-Platinum Shell Nanoparticle Electrode with a Flow Cell. J. Phys. Chem. C 2009, 113 (40), 17518-17526.

□ Recommended by ACS

Ultrafast Dynamics of Multiple Plexcitons in Colloidal Nanomaterials: The Mediating Action of Plasmon **Resonances and Dark States**

Nicola Peruffo, Elisabetta Collini, et al.

JULY 11, 2022

THE IOURNAL OF PHYSICAL CHEMISTRY LETTERS

RFAD 🗹

Impact of Vibrational Modes in the Plasmonic Purcell Effect of Organic Molecules

Dongxing Zhao, Francisco J. García-Vidal, et al.

NOVEMBER 29, 2020

ACS PHOTONICS

READ M

Effect of Ag Nanocube Optomechanical Modes on Plasmonic **Surface Lattice Resonances**

Mindaugas Juodėnas, Joel Henzie, et al.

OCTOBER 20, 2020

ACS PHOTONICS

RFAD 17

Probing the Radiative Electromagnetic Local Density of States in Nanostructures with a Scanning Tunneling Microscope

Shuiyan Cao, Elizabeth Boer-Duchemin, et al.

APRIL 24, 2020

ACS PHOTONICS

RFAD 🗹

Get More Suggestions >